

# Scanning Microscopy

---

Volume 1992  
Number 6 *Signal and Image Processing in  
Microscopy and Microanalysis*

---

Article 2

1992

## Alignment, Classification, and Three-Dimensional Reconstruction of Single Particles Embedded in Ice

Joachim Frank  
*State University of New York at Albany*

Pawel Penczek  
*Warsaw University, Poland*

Weiping Liu  
*State University of New York at Albany*

Follow this and additional works at: <https://digitalcommons.usu.edu/microscopy>



Part of the [Biology Commons](#)

---

### Recommended Citation

Frank, Joachim; Penczek, Pawel; and Liu, Weiping (1992) "Alignment, Classification, and Three-Dimensional Reconstruction of Single Particles Embedded in Ice," *Scanning Microscopy*. Vol. 1992 : No. 6 , Article 2.

Available at: <https://digitalcommons.usu.edu/microscopy/vol1992/iss6/2>

This Article is brought to you for free and open access by the Western Dairy Center at DigitalCommons@USU. It has been accepted for inclusion in Scanning Microscopy by an authorized administrator of DigitalCommons@USU. For more information, please contact [digitalcommons@usu.edu](mailto:digitalcommons@usu.edu).



## ALIGNMENT, CLASSIFICATION, AND THREE-DIMENSIONAL RECONSTRUCTION OF SINGLE PARTICLES EMBEDDED IN ICE

Joachim Frank,<sup>\*</sup><sup>1</sup> Pawel Penczek,<sup>2</sup> and Weiping Liu<sup>3</sup>

Wadsworth Center for Laboratories and Research, New York State Department of Health, Albany, NY 12201-0509

<sup>1</sup>Dept. Biomedical Sciences, State University of New York at Albany, 1400 Washington Ave., Albany, NY 12222

<sup>2</sup>Institute of Experimental Physics, Warsaw University, Warsaw, Poland

<sup>3</sup>Department of Physics, State University of New York at Albany

### Abstract

Cryo-electron microscopy of single biological particles poses new challenges to digital image processing due to the low signal-to-noise ratio of the data. New tools have been devised to deal with important aspects of 3-D reconstruction following the random-conical data collection scheme: (a) a new shift-invariant function has been derived, which promises to facilitate alignment and classification of single particle projections; (b) a new method of orientation search is proposed, which makes it possible to relate random-conical data sets to one another prior to reconstruction; and (c) the foundation is laid for a 3-D variance estimation which utilizes the oversampling of 3-D angular space by projections in the random-conical reconstruction scheme.

**Key Words:** Cryo-electron microscopy, single particles, ribosomes, 3-D reconstruction, random-conical data collection, weighted back-projection, classification using invariants, orientation search, 3-D variance distribution, significance of structural differences.

\*Address for correspondence:

Joachim Frank,  
Wadsworth Center,  
New York State Department of Health,  
Albany, NY 12201-0509

Telephone No.: (518) 474-7002  
FAX No.: (518) 474-8590

### Introduction

The random-conical reconstruction scheme (Frank et al., 1978; Radermacher et al., 1987; Radermacher, 1988), which allows 3-D images of macromolecular assemblies to be reconstructed from single-exposure electron micrographs, is now in routine use in a number of laboratories (Boisset et al., 1990; Typke et al., 1991; Carazo et al., 1988; Schroeter et al., 1991; J. Hinshaw and R. Milligan, personal communication). In contrast to other techniques proposed (e.g., Van Heel, 1987), this scheme requires no assignment of projection angles based on common lines or information of symmetries, as it is based on the more robust determination of rotation angles among comparable 0°-views. The progress in applying this technique to ice-embedded particles has been nevertheless slow because of obstacles that are either technical (the difficulty in obtaining micrographs of sufficient quality for highly [50° or above] tilted specimen grids) or intrinsic to unstained specimens (low signal-to-noise ratio [SNR]). It has become clear that new image processing tools must be developed to deal with these problems. To this end we have worked in three areas of processing associated with 3-D reconstruction: in the development of algorithms for reference-free alignment, in designing a means to orient entire random-conical projection sets with respect to each other, and in devising a general method for 3-D variance estimation. In each of these areas we are able to present some preliminary results which allow the potential of the new method to be assessed.

### A New Class of Invariants Allowing Information to be Fully Recovered

In processing electron micrographs of single particles, we are often faced with several rather dissimilar views. Some of these views may additionally vary due to some type of rocking of the molecule (e.g., Van Heel and Frank, 1981). In this situation, the alignment of the untilted projections (a prerequisite of the random-conical reconstruction) becomes a complex task. When the SNR is low, the reference image can no longer be used because of a 'bias' effect: features of the reference tend to dominate the final average, a fact that was already observed with negatively stained specimens (Boekema et al., 1986). In addi-

tion, those views which are not sufficiently similar to the reference image chosen may be left in random orientations and cannot be correctly identified. Yet another approach has been recently suggested in the general literature which takes advantage of shift-invariant properties of the bispectrum (triple correlation) (Sadler and Giannakis, 1992). Unfortunately, this method results in a rather complex algorithm and its applicability to the very noisy EM data has yet to be proven.

Recently, two methods have been proposed to solve this problem. One of these (Penczek et al., 1992) is based on a powerful reference-free alignment algorithm applied to the whole data set prior to the classification. This method performed remarkably well for the 70S ribosome particles embedded in ice. It is likely that its application can be extended to many other kinds of particles which have projections with similar overall shape. However, it is not clear how this method would perform for distinctly different views, for example, a mixture of round and rectangular shapes, particularly in the presence of high noise. The other method (Schatz and van Heel, 1990), takes advantage of translation- and rotation-invariant functions (so-called double auto-correlation functions) derived from the raw images. These invariants can be subjected to multivariate statistical analysis (MSA) and classification prior to the alignment. The particular advantage of invariants is that a large set of images can be split into more homogenous groups, thereby simplifying the subsequent alignment. The main problem associated with the particular choice of the invariant functions suggested by these authors is the double elimination of the phase information. This part of the Fourier representation of an image is largely responsible for the shape and interior structure of a particle image, and its loss may degrade the classification, lumping entirely different particles into the same class.

In the following we will derive new shift-invariant functions that do preserve the non-trivial part of the Fourier phase information, and we will discuss some results obtained from simulated data. We will also discuss the possibility of extending the method proposed to obtain functions that are both translation- and rotation-invariant yet still preserve the full Fourier information.

The circular shift of a discrete series  $f_n$  is defined by

$$f'_n = f_{(n+m) \pmod N}, \quad n=0,1, \dots, N-1 \quad (1)$$

where  $m$  is the shift and  $N$  is the length of the series. The same shift can be applied in Fourier space by:

$$F'_k = F_k \exp(-2\pi i \frac{m}{N} k) \quad (2)$$

where complex numbers  $F_k$  represent the discrete Fourier transform of  $f_n$ . If we define the phase corresponding to the shift by

$$2\pi \frac{m}{N} = \eta \quad (3)$$

and use the modulus-phase representation of complex numbers  $F_k$ :

$$F_k = \rho_k \exp(i\phi_k) \quad (4)$$

where  $\rho_k = |F_k|$  is the modulus and  $\phi_k = \arg(F_k)$  is the argument (phase), we see that the shift given by (1) is defined in Fourier space by

$$F'_k = \rho_k \exp(i(\phi_k + k\eta)) \quad (5)$$

which means that the moduli of Fourier representation are not affected by the shift and that the phases of the shifted image are modified according to

$$\phi'_k = \phi_k + k\eta, \quad k=1, \dots, N/2 \quad (6)$$

(for a real-valued series  $f_n$  the zero-term phase  $\phi_0$  is equal to zero).

We define a set of 1-D shift-invariants as follows:

$$v_2 = \phi_2 - 2\phi_1 \quad (7)$$

$$v_k = \phi_k - \phi_{k-1} - \phi_{k-2} + \phi_{k-3}, \quad k=3, \dots, N/2$$

It can be verified that the terms  $v_k$  do not depend on the shift applied to the series. The phases  $\phi_k$  can be easily retrieved from the invariants  $v_k$  by choosing a value for the first phase  $\phi_1$  and inverting equation (7). This corresponds to a choice of initial shift of the entire series and means that no information about the "shape" of the function is lost.

A similar reasoning can be applied to the 2D case. The 2D circular shift is described by the following modification of the phases of the Fourier representation:

$$\phi'_{kl} = \phi_{kl} + k\eta + l\psi \quad (8)$$

$$k=0,1, \dots, N/2; \quad l=0,1, \dots, L/2$$

The shift-invariants in the 2-D case are defined by:

$$v_{kl} = \phi_{kl} - \phi_{k-1,l} - \phi_{k,l-1} + \phi_{k-1,l-1} \quad (9)$$

$$k=1, \dots, N/2; \quad l=1, \dots, L/2$$

It can be easily verified that the terms  $v_{kl}$  do not depend on shift. To code all the phase information eq. (7) should be applied to phases  $\phi_{k,0}$  and  $\phi_{0,l}$ . Similarly, as in the 1-D case, the number of coefficients is reduced: two phases are now redundant ( $\phi_{1,0}$  and  $\phi_{0,1}$ ) since they describe the initial shift of the discrete image in two perpendicular directions.

To test the proposed shift-invariant representation we created a test image of size 64x64

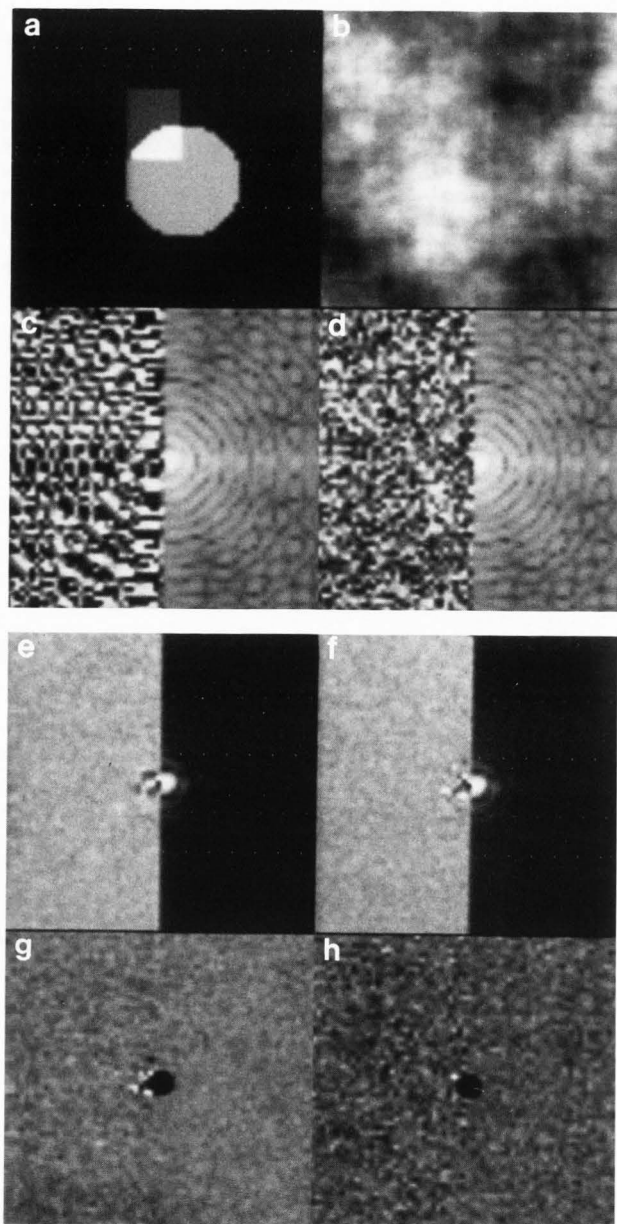


(Fig. 1a). The second test image (Fig. 1b) was created from the first one by scrambling the phases and preserving the moduli of its Fourier transform. Thus, both images have exactly the same power spectrum and differ by the phase information only. Figs. 1c and 1d show phase-invariants (left half of each square) and power spectra (right half of each square) for both test images. (For the purpose of the display the logarithms of the power spectra are shown). Each test image was randomly shifted by non-integer circular shifts (using Fourier interpolation) ranging from 0.0 to 64.0 and Gaussian noise with average zero and standard deviation one was added. Thus, from each test image we obtained 100 randomly shifted copies with SNR ranging between 1 and 3. In the next step the power spectra and phase-invariants were calculated for each image. The averages of both sets are shown in Figs. 1e and 1f. We note that within the

Fig. 1. Test of shift-invariant representation of 2D images.

- (a) Test image of size 64x64.
- (b) Second test image created from the first in (a) by scrambling the phases and preserving the moduli of its Fourier transform.
- (c) Phase-invariants (left half of the image) and logarithm of power spectrum (right half of the image) of test image (a).
- (d) Phase-invariants (left half of the image) and logarithm of power spectrum (right half of the image) of test image (b).
- (e) Average of 100 shift-invariants obtained from test image (a) by applying random shifts and adding Gaussian noise (SNR ranging between 1 and 3).
- (f) Average of 100 shift-invariants obtained from second test image in (b) by applying random shifts and adding Gaussian noise (SNR ranging between 1 and 3).
- (g) First eigen-image obtained by applying MSA to the 200 shift-invariant images.
- (h) Second eigen-image obtained by MSA above.

central region where the power spectrum has appreciable values, the averaged phase-invariant function has a distinct pattern.

The 200 images were subjected to MSA. The first two eigen-images obtained are shown in Figs. 1g and 1h. None of them contains any information in the right half corresponding to the power spectra - this is understandable since the power spectra were identical for all the images processed. The left half of the first eigenimage (Fig. 1g) contains close to the center recognizable pattern similar to the pattern observed in the averages (Figs. 1e and 1f). Thus, this first factor was used in a hierarchical clustering program with complete linkage as merging criterion. The two classes obtained agree in 85% of all cases with the known origin of the images.

To obtain a rotation-invariant representation of the image, we can express the image in polar coordinates and calculate the Fourier transforms along circles. These 1-D Fourier transforms can be represented by their moduli and, using eq. (7), by their 1-D phase-invariants. It is still an open question how the two approaches (i.e., for obtaining a translational-invariant and rotation-invariant representation) can be combined to create a fully invariant representation of an image.

#### Global Orientation Search Among Projection Data Sets

The problem of determining the relative orientations of three-dimensional structures from their two-dimensional projections has two known solutions: the so-called common lines approach and the method of moments. The first, originally proposed by Crowther et al. (1970), is routinely used in the 3D reconstruction of virus structures with high symmetry and was later extended to general non-symmetrical structures (Goncharov, 1986; Van Heel, 1987). The second method (Goncharov, 1986; Salzman, 1990), with its high sensitivity to errors in the data, is of rather academic interest.

In the framework of the random-conical 3D reconstruction of non-symmetrical particles (Radermacher et al., 1987; Radermacher, 1988) the

problem of orientation determination is automatically solved: the random-conical scheme of data collection provides all the Eulerian angles required for the 3D reconstruction. Two of these angles are determined with high accuracy from the tilt geometry and the third one is found through the alignment of particles from the untilted-specimen micrograph. Provided that the structure occurs on the specimen grid in a preferred orientation, its 0-degree projections differ only by a rotation in the plane of the grid, and the corresponding angles can be found using the alignment procedure. The important advantage of this approach is that only the presumably identical projections are compared and the resulting average has high SNR, which facilitates the determination of the missing third Eulerian angle with high accuracy. Reconstructions obtained in this way are however limited by the missing angular region, and efforts must be made to fill this region using more than one preferred orientation. Therefore the problem of orientation determination resurfaces, but this time it can be solved by relating entire data sets to one another.

In our recent reconstruction of the 70S *Escherichia coli* ribosome (Frank et al., 1991; Penczek et al., 1992) we took advantage of a number of preferred orientations in which this particle can be found. After calculating separate 3D reconstructions for three different 50-degree tilt data sets, we applied a search in real space directly to the reconstructed volumes in order to determine the relative orientations of the structures. This approach proved to be successful and we were able to calculate a "merged reconstruction" combining all three data sets. Due to the span of the particular orientations used, the angular coverage of this merged reconstruction was virtually complete. However, this method relies on the availability of high-tilt data, and special care must be taken to at least partially recover the missing cone information in each individual reconstruction, so as to minimize bias in the orientation search.

To overcome these problems, we would like to put forward another method of determining the orientation between the tilted data. Instead of finding the orientation between two reconstructions, we find the best match between the two corresponding sets of input projections, assuming the geometry within each set (in terms of Eulerian angles of each projection) is known. (There is certain analogy between our method and Crowther's (1971) use of multiple common line that occur when comparing arbitrary projections of two highly symmetric virus particle. However, the differences between the two methods are obvious: we compare entire sets of particles with each other, and the projections within each set are tied together not by symmetry but by a common reference system, which is established by the alignment of the 0-degree views.)

Since our projection data are collected within the framework of the random-conical scheme, the Fourier transforms of the projections form a set of planes in Fourier space tangential to the cone. Thus, the problem of finding the orientation between two 3D structures can be formulated as the problem of finding the best matching orientations between two such sets of Fourier planes tangential to their respective cones.

Any two planes intersect in 3D along a single

line (except in the degenerated case in which they coincide), the common line. Along this line we wish to calculate the discrepancy  $1-\rho_{12}$ , where  $\rho_{12}$  is the correlation coefficient calculated along this line. To find the direction of the common line with respect to the two planes, we proceed as follows: we assume that the orientations of the planes in the coordinate systems associated with their cones are given by rotation matrices  $R_1$  and

$R_2$ , respectively<sup>1</sup>. We further assume that the relative orientation between the two sets of planes (or two cones) is given by the rotation matrix  $R_T$ . The directions of the intersection line are given by the solution to the following set of equations:

$$R_1^{-1} n_1 = R_T^{-1} R_2^{-1} n_2 \quad (10)$$

where

$$n_k = \begin{pmatrix} \cos \alpha_k \\ \sin \alpha_k \\ 0 \end{pmatrix} \quad k=1,2 \quad (11)$$

are the unitary vectors defining the orientation of the line on corresponding planes. To solve the system of equation (10) for two unknown angles  $\alpha_1$  and  $\alpha_2$  we have to replace the product of three rotation matrices  $R_2 R_T R_1^{-1}$  by the new rotation matrix  $R$  and solve the simpler problem

$$R n_1 = n_2 \quad (12)$$

The solution is given by

$$\begin{aligned} \alpha_1 &= 90 + \phi \\ \alpha_2 &= 90 - \psi \end{aligned} \quad (13)$$

The angles  $\phi$  and  $\psi$  are functions of the Eulerian angles describing the orientation of both planes in their own system of coordinates as well as the parameter angles describing the relative orientation between the two structures. The explicit equations are not needed since these angles can be easily retrieved from the elements of the rotation matrix  $R$ .

1. Our convention in the use of Eulerian angles is according to the following definition of the rotation matrix

$$R(\psi, \theta, \phi) = R_1(\psi) R_2(\theta) R_3(\phi) = \begin{pmatrix} \cos \psi & \sin \psi & 0 \\ -\sin \psi & \cos \psi & 0 \\ 0 & 0 & 1 \end{pmatrix} \begin{pmatrix} \cos \theta & 0 & -\sin \theta \\ 0 & 1 & 0 \\ \sin \theta & 0 & \cos \theta \end{pmatrix} \begin{pmatrix} \cos \phi & \sin \phi & 0 \\ -\sin \phi & \cos \phi & 0 \\ 0 & 0 & 1 \end{pmatrix}$$

### 3-D reconstruction of ice-embedded single particles

**Table 1.** Eulerian angles ( $\phi$ ,  $\theta$ ,  $\psi$ ) describing the 3D orientation found between three pairs of 70S ribosomes data sets.

Rotated structure	Reference structure	
	I	II
II	$\phi = 91.7 \quad \theta = 67.4 \quad \psi = -41.5^a$ $\phi = 93.0 \quad \theta = 71.4 \quad \psi = -39.6^b$	
III	$\phi = 90.6 \quad \theta = 75.5 \quad \psi = -35.9^a$ $\phi = 90.0 \quad \theta = 79.8 \quad \psi = -34.3^b$	$\phi = 235.9 \quad \theta = -12.8 \quad \psi = 119.5^a$ $\phi = 235.7 \quad \theta = -10.5 \quad \psi = 120.8^b$

<sup>a</sup>calculated by the orientation search in the space of Fourier planes directly from the projection data;

<sup>b</sup>calculated in the real space by the maximization of correlation coefficient between reconstructed 3D volumes.

We defined the global discrepancy between two sets of planes in the following way:

$$D(I, II; R_T) = \sum_{m_1=1}^{M_1} \sum_{m_2=1}^{M_2} (1 - \rho(m_1, m_2)) \quad (14)$$

where  $M_1$  and  $M_2$  are the numbers of projections (or Fourier planes) in structures I and II, respectively, and  $\rho(m_1, m_2)$  is the correlation coefficient calculated along the intersecting line between planes belonging to the first and second structure. The directions of the line are given by equation (13).

The best matching orientation is defined by the rotation matrix  $R_T$  for which the global discrepancy in equation (14) is minimized. To find this minimum, one of the standard procedures may be used such as the minimization procedure implemented in the IMSL package (IMSL, 1987), which is based on a quasi-Newton method using finite-difference gradient.

To test the method described, we used the already reconstructed 70S *Escherichia coli* (E. coli) ribosome structure (Penczek et al., 1992) filtered to  $1/40 \text{ \AA}^{-1}$  as noise-free model. From this model, we created 36 projections in 10 degrees steps at 50 degrees tilt. The second set of 36 projections was created after arbitrary rotation of the structure by the three Eulerian angles. Using the new orientation program described, we were able to calculate the correct angles from the projection data within one degree accuracy. In the second test, we created the same number of projections, but at 30 degrees tilt. Again, there was no difficulty in finding the correct angles.

In a third test, we applied the new procedure to an experimental set of projections. We used the three sets of 50-degree tilt data of the 70S E. coli ribosome belonging to different zero-degree views, as described in (Penczek et al., 1992). The number of projections in the respective sets were 69, 93, and 66. Using the global orientation search, we calculated the Eulerian angles between each pair of projection sets. The results are listed in Table 1. For comparison, we also listed the Eulerian angles resulting from the previous calculations done in real space by maximization of the correlation coefficient between two reconstructed 3D volumes (for details see Penczek et al., 1992).

Both sets of results agree to a large extent. The solutions differ mostly in the values of  $\theta$  angles. This discrepancy can be explained by the bias of the search in real space (results denoted by (b)) caused by the missing cone.

The proposed method of determination of the relative orientations of three-dimensional structures by a search directly in the space of projection data has numerous advantages. The determination of Eulerian angles can be done prior to the actual 3D reconstruction. The collection of well-behaved high-tilt data (at 50 degrees or above), which is extremely time-consuming and appears to be a major technical obstacle in the attempts to reconstruct single particles embedded in ice, is no longer required. Our experiments showed that tilts as low as 30 degrees should be sufficient. Such lower tilt of the specimen means that the defocus spread across the micrograph is reduced, which in turn increases the size of the useful image field. And finally, provided that the particle occurs on the specimen grid in a sufficient number of preferred orientations to cover the entire angular range, the resulting merged reconstruction will be free of the missing-cone problem, which causes distortions in any individual reconstruction.

Currently we are working on an application of the method described to improve the resolution of the reconstruction of ice-embedded 70S E. coli ribosome. Our previous work (Frank et al., 1991) has shown that at least seven different orientations are assumed by this particle.

#### The 3-D Variance of Weighted Back-Projection Principle of Variance Estimation

When two independent reconstructions of related particles (e.g. labeled vs. unlabeled) are compared, the following questions are raised: could they have arisen from the same structure?; where are the feature differences located?; how reliable are the conclusions? These questions can be answered by estimating the variances of the 3-D reconstructions. Earlier controversies in the literature (Hegerl and Hoppe, 1976; Saxberg and Saxton, 1981; Hoppe and Hegerl, 1981; Van Heel, 1986) about the effect of quantum noise on the reconstruction can also be solved on the basis of our variance estimate.

To establish the definition of 3-D variance and the theoretical relationship between the 3-D variance and the projection noise, a "gedankenexperiment" is designed: for a given set

of  $N$  view angles, we get a set of  $N$  projections, and from this the corresponding 3-D weighted back-projection reconstruction is computed. Suppose we can get many such sets of projections independently for the same set of view angles, and compute their reconstructions. Then, because of the propagation of projection noise, these reconstructions will be different due to their noise components. The variation of the noise components among the "gedanken" reconstructions gives the definition of variance of the 3-D reconstruction.

Based on this definition of 3-D variance, starting from the same sampled and aligned projection set for 3-D reconstruction and tracing along the route of reconstruction, a theoretical relationship between the 2-D variances of the projections and the 3-D variance of the reconstruction is first established. From noise information hidden in the "surplus" number of projections (relative to Shannon's sampling requirement applied to the sampling of the 3-D Fourier transform), noise levels of each projection are estimated by comparing it with neighbor projections. The 3-D variance estimate is subsequently calculated from the projection noise estimates. It is important to note that it is the linear and shift-invariant property of the weighted back-projection algorithm that makes such tracing of noise propagation possible. A preliminary report of this work has been given by Liu (1991).

#### The 3-D Variance Estimation Algorithm

In the analysis below, we made use of the following definitions:

$I(\vec{r})$ : projection interpolation function.

$P^{(i)}(k, l)$ : digitized and centered projection number  $i$ .

$W^{(i)}(\vec{r})$ : inverse FT of the weighting function of projection  $i$ .

(The weighting functions for a projection set with arbitrary projection orientations can be found in Radermacher et al., 1986 and Harauz and Van Heel, 1986.)

$F(\vec{R})$ : inverse FT of 3-D resolution filtration function; its projections:  $F^{(i)}(\vec{r})$ .

Convolution of a sampled function, for example  $P^{(i)}(k, l)$ , with a continuous function is understood to mean:

$$\sum_{k, l} P^{(i)}(k, l) \delta(r - (k, l)).$$

The weighted back-projection reconstruction algorithm can be expressed as:

$$\begin{aligned} B(\vec{R}) &\equiv \\ &\sum_{i=1}^N \text{BP} [P^{(i)}(k, l) \circ I(\vec{r}) \circ W^{(i)}(\vec{r})] \circ F(\vec{R}) \\ &= \sum_{i=1}^N \text{BP} [P_{i\text{wf}}^{(i)}(\vec{r})] \end{aligned} \quad (15)$$

where the weighted projection is defined as:

$$\begin{aligned} P_{i\text{wf}}^{(i)}(\vec{r}) &\equiv \\ &P^{(i)}(k, l) \circ I(\vec{r}) \circ W^{(i)}(\vec{r}) \circ F^{(i)}(\vec{r}) \\ &= P^{(i)}(k, l) \circ H_{i\text{wf}}^{(i)}(\vec{r}) \end{aligned} \quad (16)$$

with:

$$H_{i\text{wf}}^{(i)}(\vec{r}) \equiv I(\vec{r}) \circ W^{(i)}(\vec{r}) \circ F^{(i)}(\vec{r}) \quad (17)$$

Now we define the projection noise:

$$N^{(i)}(k, l) \equiv P^{(i)}(k, l) - \overline{P^{(i)}(k, l)} \quad (18)$$

(upper bar here and in the following denotes ensemble average). So the weighted projection noise is:

$$\begin{aligned} N_{i\text{wf}}^{(i)}(\vec{r}) &\equiv P_{i\text{wf}}^{(i)}(\vec{r}) - \overline{P_{i\text{wf}}^{(i)}(\vec{r})} \\ &= N^{(i)}(k, l) \circ H_{i\text{wf}}^{(i)}(\vec{r}) \end{aligned} \quad (19)$$

Since different projections come from different particles on the grid, the noise  $N_{i\text{wf}}^{(i)}(\vec{r})$  is uncorrelated between projections, and the variance of the 3-D reconstruction as a function of the projection noise level is:

$$\begin{aligned} V(\vec{R}) &\equiv [B(\vec{R}) - \overline{B(\vec{R})}]^2 = \\ &\sum_{i=1}^N \text{BP} \{ [N_{i\text{wf}}^{(i)}(\vec{r})]^2 \} \end{aligned} \quad (20)$$

where BP means back-projection operation.

The neighbor projections ( $i-\delta$  to  $i+\delta$ ) are used for the noise estimation of projection  $i$  ( $\delta = \frac{1}{2}, 1, \frac{3}{2}, 2, \dots$ ; round-off of  $i-\delta$  and  $i+\delta$  is implied when  $\delta$  is a half-integer),

$$\begin{aligned} \tilde{N}^{(i)}(k, l) &\equiv \\ &\sqrt{\frac{2\delta+1}{2\delta}} [P^{(i)}(k, l) - \frac{1}{2\delta+1} \sum_{j=i-\delta}^{i+\delta} P^{(j)}(k, l)] \end{aligned} \quad (21)$$

$$\tilde{N}_{i\text{wf}}^{(i)}(\vec{r}) \equiv \tilde{N}^{(i)}(k, l) \circ H_{i\text{wf}}^{(i)}(\vec{r}) \quad (22)$$

The 3-D variance estimation is thus established by

$$\tilde{V}(\vec{R}) \equiv \sum_{i=1}^N \text{BP} \{ [\tilde{N}_{i\text{wf}}^{(i)}(\vec{r})]^2 \} \quad (23)$$

### 3-D reconstruction of ice-embedded single particles

Since the computer cannot process continuous functions,  $[\tilde{N}_{wf}^{(i)}(\vec{r})]^2$  is computed at discrete pixels, and interpolation has to be used in its back-projection operation. Practically, the sampling rate of  $(k,l)$  is  $5 \text{ \AA}$ , while  $\tilde{N}^{(i)}(k,l)$  is low-pass filtered by  $F^{(i)}(\vec{r})$  to around 30 to 40  $\text{\AA}$ , which is the resolution of a typical reconstruction, so even without padding, the error caused by this interpolation procedure can still be small. Hence the practical 3-D variance estimate is:

$$\tilde{V}(\vec{R}) \approx \sum_{i=1}^N \text{BP} \{ [\tilde{N}_{wf}^{(i)}(k,l)]^2 \circ I(\vec{r}) \} \quad (24)$$

where

$$\tilde{N}_{wf}^{(i)}(k,l) \equiv \tilde{N}^{(i)}(k,l) \circ H_{wf}^{(i)}(k,l) \quad (25)$$

with:

$$H_{wf}^{(i)}(k,l) \equiv W^{(i)}(k,l) \circ F^{(i)}(k,l) \quad (26)$$

#### Estimation of Error Due to Signal Variation

In attributing all variations among neighbor projections to noise, we are neglecting the variations due to the signal component. In the following, an upper bound for the resulting error in the 3D variance estimate is given.

The main difference among neighbor signal components arises from the peripheral part of the object's structure. The most drastic change is observed when we regard a point at distance  $D/2$  from the center of the object, where  $D$  is the object's diameter. Let us assume that there is an  $m$ -fold over-sampling at the cut-off frequency in 3-D Fourier space, which corresponds to an  $m$ -fold "surplus" of projections. For such a model, the ratio of the signal component difference to the noise component difference can be derived as:

$$\frac{\text{VAR} [\tilde{N}_{sf}^{(i)}(\vec{r})]}{\text{VAR} [\tilde{N}_{nf}^{(i)}(\vec{r})]} \leq 41.6 * (\text{SNR}) / m'^4 \quad (27)$$

for  $m' \gg 1$

with SNR being the signal-to-noise ratio of projections after resolution filtration to the same level as used for the variance estimates, and  $m'$  being the fold of over-sampling when neighbor projections are only counted. It can be shown that  $m=2m'$  on the average for the conical tilt series.

Practically, to minimize the error caused by such signal component differences, immediate neighbor projections ( $\delta=1/2$  or 1) are used for comparison.

#### Significance Assessment of Structural Differences of Related Reconstructions

Let  $B_1(\vec{R})$  and  $B_2(\vec{R})$  be two independent reconstructions. The noise components of the two reconstructions at any  $\vec{R}$  are roughly Gaussian-distributed. This assumption is justified because the reconstruction noise component at  $\vec{R}$  is the

summation of a large number of independent projection noise components. If we assume their variance estimates  $\tilde{V}_1(\vec{R})$  and  $\tilde{V}_2(\vec{R})$  to have  $\chi^2$ -distributions with  $N_{e1}$  and  $N_{e2}$  degrees of freedom, respectively, that is:

$$\text{VAR} [\tilde{V}_i(\vec{R})] = \frac{1}{N_{ei}} V_i^2(\vec{R}) \quad (28)$$

The condition of equal variances (Dudewicz and Mishra, 1988) is in this case equivalent to:

$$(N_{e1}+1) V_1^2(\vec{R}) = (N_{e2}+1) V_2^2(\vec{R}) \quad (29)$$

Then for such a comparison of two empirical means from equivalent population sizes of  $(N_{e1}+1)$  and  $(N_{e2}+1)$ , provided that

$$\frac{N_{e1}}{N_1} = \frac{N_{e2}}{N_2} \quad (30)$$

(which holds when the neighbor projections are compared in the same way for the two 3-D variance estimates), the test statistic becomes (Dudewicz and Mishra, 1988):

$$\hat{t}(\vec{R}) = \frac{|B_1(\vec{R}) - B_2(\vec{R})|}{\sqrt{\frac{N_1}{N_2} \tilde{V}_1(\vec{R}) + \frac{N_2}{N_1} \tilde{V}_2(\vec{R})}} \quad (31)$$

If  $\hat{t}(\vec{R}) > t_{N_{e1}+N_{e2}, \alpha}$ ,  $B_1(\vec{R}) \neq B_2(\vec{R})$  is significant at the 100 $\alpha\%$  level.

In practical 3-D reconstructions, the numbers of projections  $N_i$  are  $>30$ , and from the analysis of variance of the variance estimate, it can be shown that  $N_{ei} \approx N_i/2$ , so  $N_{e1} + N_{e2} > 30$ . The  $t$ -distribution  $t_{v, \alpha}$  is therefore approximately equal to the standard normal distribution  $n_\alpha$  (Sachs, 1984), so  $n_\alpha$  can be used for  $t_{v, \alpha}$  in above statistical test, which avoids having to estimate  $N_{e1}$  and  $N_{e2}$ .

Implicitly, the application of the resolution filtration to the projections (see Section on 3-D Variance Estimation Algorithm) produces a variance estimate relating to a local average over a sphere of diameter  $1/(2r_{fc}^*)$  if  $r_f^* = r_{fc}^*$  is the resolution cutoff according to Crowther et al. (1971). The test in eq. (31) therefore relates to the reproducibility of averaged features within such a sphere.

It is immediately clear that the variance contributions are strongly spatial frequency dependent, due to the different sampling densities in different spatial frequency bands, with the sampling getting finer as we decrease the cutoff frequency. As a result of this geometrical condition, different choices of cutoff frequency in the filtration function (i.e., values smaller than

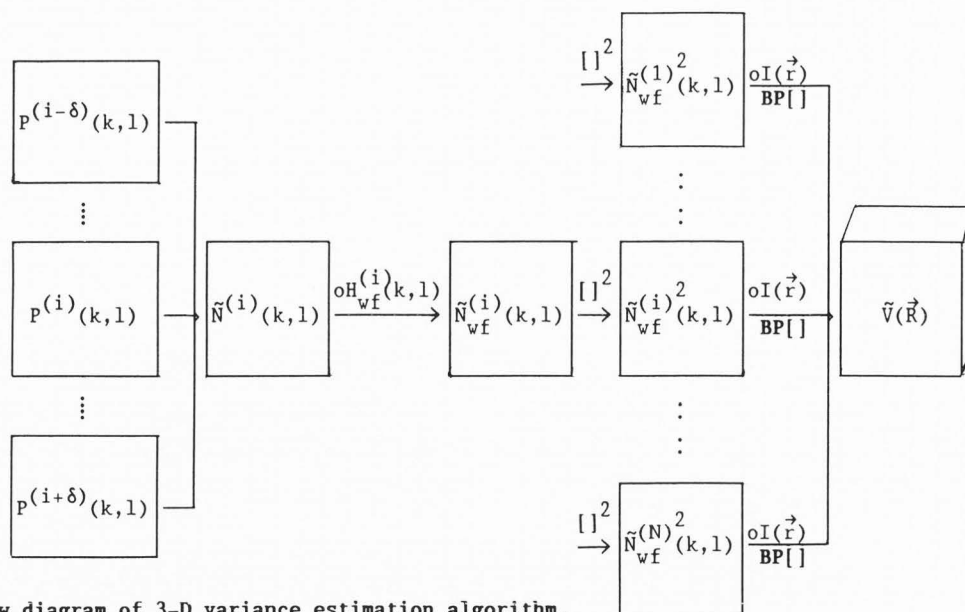


Fig. 2. Flow diagram of 3-D variance estimation algorithm.

$r_{fc}^*$  produce somewhat different (although largely consistent) answers in the t-test (31): not only does the pattern of highly significant differences change, but the significance level also increases as the filtration radius  $r_f^*$  is being decreased.

It is therefore useful to apply the t-test to a number of different variance estimates obtained by using different  $r_f^*$ 's, to "tune in" on the variability of features in different size ranges. [Note that this is not equivalent to the result of a low-pass filtration of the 3D variance map, which does not have a meaning in the framework of this analysis.]

#### Practical Procedure of Structural Comparisons

The results from the theoretical analysis of 3D variance estimation suggests the following procedure in assessing the significance of 3D structural differences: Suppose we have projection sets A and B. They can be (a) from particles in different conformational states, separated by MSA and classification of  $0^\circ$  projections, (b) from two different preparation techniques of the same particle, or (c) from an experiment in which the particle-ligand complex is compared with the particle itself. The important feature these experiments have in common is that they lead to two classes representing structurally similar particles, so that they can be meaningfully aligned according to their common features.

We first compute the 3-D reconstructions of A and B, and then follow the back-projection pathway (Fig. 2) to compute the 3-D variances of A, B and the mixed set (A+B) for different  $r_f^*$ .

There are two ways in which we can use this information:

(a) we can study the difference map of the two reconstructions, in combination with the quantitative significance assessment of such differences from their 3-D variances.

(b) as a complementary way, which is qualita-

tive and visually more comprehensible, we can compare the 3-D variance map of the mixed set with that of each set. If a highlight is shown in the 3D variance of (A+B) but not in those of either A or B, we can say that at this spot the structural difference of A and B is significant.

As a first test of this variance estimation scheme (Liu, 1991), we have analyzed the data set of Carazo et al. (1988) which comprises 946 projections of the 50S ribosomal subunit depleted of proteins L7/L12 (Fig. 3). Although this specimen was prepared by using negative staining, it nevertheless illustrates the potential of 3-D variance estimation in assessing significance of structural differences.

#### Conclusions

New tools have been described which promise to facilitate the 3-D reconstruction of ice-embedded single biological particles. While these tools have been designed as part of a continuing strife to extend the application field of the random-conical reconstruction scheme, both the new shift invariant and the mechanism of 3-D variance estimation potentially have a much wider field of application.

The list of problems requiring attention is of course much longer. Among the unsolved problems are (a) a way of quantitatively refining the angle assignments to account for particle rocking; (b) a satisfactory approach toward transfer function correction and disentanglement of elastic and inelastic signal; and (c), closely connected to the latter point, the use of differently defocused micrographs to obtain higher resolution (in the 10-15 Å-range). Finally, thinking about the extended automation and control capabilities of the new generation of electron microscopes, we could pose the question to what extent the instrument can be employed to perform some of the complex tasks of data collection, prescreening, and windowing of particles (see first efforts in this area and the related area of electron tomography by Typke et al., 1990; 1991).

# 3-D reconstruction of ice-embedded single particles

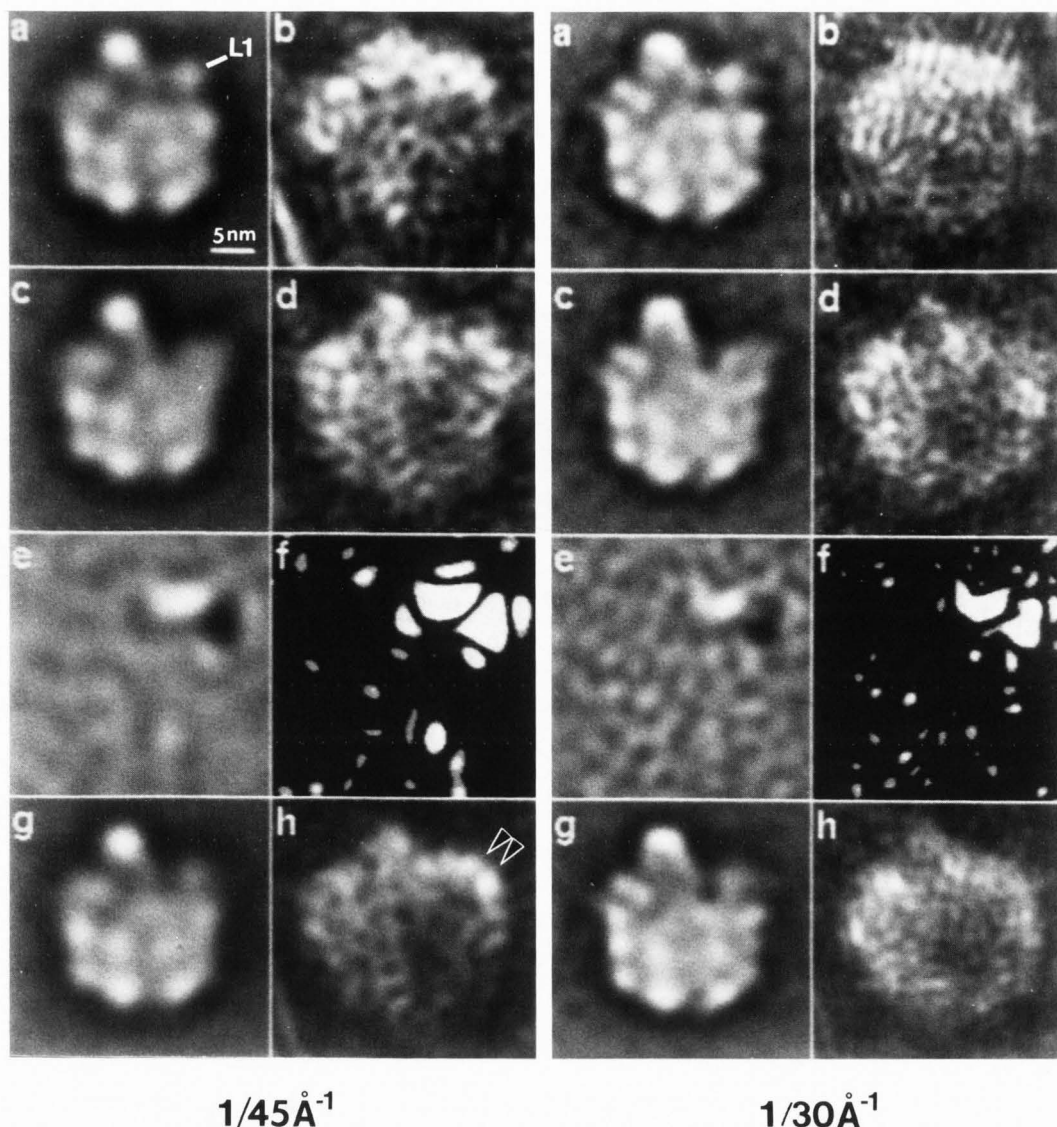


**Fig. 3.** Significance assessment of differences between two reconstructions. The data from *E. coli* 50S ribosomal subunits depleted selectively of proteins L7/L12 (Carazo *et al.*, 1988) were used. The two projection sets were obtained by classifying the projections via MSA.

All calculations were duplicated with different frequency cutoffs  $r_f^* = 1/45 \text{ \AA}^{-1}$  and  $r_f^* = 1/30 \text{ \AA}^{-1}$ .

(a) Central section of the weighted back-projection reconstruction of Class I. Number of projections  $N_1 = 196$ .

(b) Variance estimation map of the reconstruction of Class I as shown in (a).

(c) Central section of the reconstruction of Class II.  $N_2 = 225$ .

(d) Variance estimation map of the reconstruction of Class II as shown in (c).

(e) Difference map from the reconstructions of Class I and II as shown in (a) and (c).

(f) Significance map of the differences as shown in (e). Bright areas correspond to the level of significance  $\alpha = 99\%$  where  $\hat{t}(\vec{R}) > n_{0.01}$ , while bright and grey areas correspond to  $\alpha = 95\%$  where  $\hat{t}(\vec{R}) > n_{0.05}$ .

(g) Central section of the reconstruction of the mixed Class (I+II).

(h) Variance estimate of the reconstruction of Class (1+2) as shown in (g). The granularity of the map is due to the statistical behavior of the 3-D variance estimate. The two maxima in the L1 region stand out from the granular background, reflecting the structural difference between the two classes which is due to the "waving" of the L1 shoulder of the particle.

# Acknowledgements

This work was supported by grants NIH 1R01 GM 29169, 1S10 RR 03998, and NSF 8721474.

# References

- Boekema E.J., Berden J.A., and van Heel M. (1986). Structure of mitochondrial F1-ATPase studied by electron microscopy and image processing. *Biochem. Biophys. Acta* 957, 370-379.
- Boisset N., Taveau J.-C., Lamy J., Wagenknecht T., Radermacher M., and Frank J. (1990). Three-dimensional reconstruction of native *Androctonus australis* hemocyanin. *J. Mol. Biol.* 216, 743-760.
- Carazo J.M., Wagenknecht T., Radermacher M., Mandiyan V., Boublik N., Frank J. (1988). Three-dimensional structure of 50S *Escherichia coli* ribosomal subunits depleted of proteins L7/L12. *J. Mol. Biol.* 201, 393-404.
- Crowther R.A., DeRosier D.J., Klug A. (1970). The reconstruction of a three-dimensional structure from projections and its application to electron microscopy. *Proc. Roy. Soc. Lond. A* 317, 319-340.
- Crowther R.A. (1971) Procedures for three-dimensional reconstruction of spherical viruses by Fourier synthesis from electron micrographs. *Phil. Trans. Roy. Soc. Lond. B* 261, 221-230.
- Dudewicz E.J., Mishra S.N. (1988) *Modern Mathematical Statistics*. Wiley Series in Prob. and Math. Statistics, New York.
- Frank J., Goldfarb W., Eisenberg D., and Baker T.S. (1978). Reconstruction of glutamine synthetase using computer averaging. *Ultramicroscopy* 3, 283-290.
- Frank J., Penczek P., Grassucci R., Srivastava S. (1991). Three-dimensional reconstruction of the 70S *Escherichia coli* ribosome in ice: the distribution of ribosomal RNA. *J. Cell Biol.* 115, 597-605.
- Goncharov A.B. (1986). Methods of integral geometry and three-dimensional reconstruction of objects. Preprint of Cybernetic Council Acad. Sci. (in Russian).
- Hegerl R., Hoppe W. (1976). Influence of electron noise on three-dimensional image reconstruction. *Zeitschrift für Naturforsch* 31a, 1717-1721.
- Hegerl R., Hoppe W. (1981). Some remarks concerning the influence of electron noise on 3D reconstruction. *Ultramicroscopy* 6, 205-206.
- Harauz G., Van Heel M. (1986). Exact filters for general geometry three dimensional reconstruction. *Optik* 73, 146-156.
- IMSL (April 1987). User's Manual, Version 1.0.
- Liu W. (1991). 3-D variance of weighted back-projection reconstruction and its application to the detection of 3-D particle conformational changes. *Proc. 49th Ann Meetg. Electron Microscopy Society of America*, G.W. Bailey, ed., San Francisco Press, Inc., 542-543.
- Penczek P., Radermacher M., and Frank J. (1992). Three-dimensional reconstruction of single particles embedded in ice. *Ultramicroscopy* 40, 33-53.
- Radermacher M., Wagenknecht T., Verschoor A., Frank J. (1986). A new 3D reconstruction scheme applied to the 50S ribosomal subunit of *E. coli*. *J. Microscopy* 141, RP1-RP2.
- Radermacher M., Wagenknecht T., Verschoor A., Frank J. (1987). Three-dimensional reconstruction from a single-exposure random conical tilt series applied to 50S ribosomal subunit of *Escherichia coli*. *J. Microsc.* 146, 113-136.
- Radermacher M. (1988). Three-dimensional reconstruction of single particles from random and nonrandom tilt series. *J. of Electron Mic. Tech.*, 9, 359-394.
- Sachs L. (1984). *Applied Statistics*, A Handbook of Techniques. Springer-Verlag, New York.
- Sadler B.M., Giannakis G.B. (1992). Shift- and rotation-invariant object reconstruction using the bispectrum. *J. Opt. Soc. Am. A* 9, 57-69.
- Salzman D.B. (1990). A method of general moments for orienting 2D projections of unknown 3D objects. *Computer vision, graphics, and image processing* 50, 129-156.
- Schatz M. and van Heel M. (1990). Invariant classification of molecular views in electron micrographs. *Ultramicroscopy* 32, 255-264.
- Schroeter J.P., Wagenknecht T., Kolodziej S.J., Bretauiere J.-P., Strickland D.K., and Stoops J.K. (1991). Three-dimensional structure of the chymotrypsin-human  $\alpha_2$ -macroglobulin complex. *FASEB Journal* 5, A452.
- Typke D., Pfeifer G., Hegerl R., and Baumeister W. (1990). 3D reconstruction of single particles by quasi-conical tilting from micrographs recorded with dynamic focusing. *Proc. XII Intl. Congress for Electron Microscopy*, L.D. Peachey and D.B. Williams, eds., San Francisco Press, Inc., Vol I, 244-245.
- Typke D., Dierksen K., and Baumeister W. (1991). Automatic tomography. *Proc. 49th Ann. Meetg. Electron Microscopy Society of America*, G.W. Bailey, ed., San Francisco Press, Inc., 544-545.
- Van Heel, M. and Frank, J. (1981) Use of multivariate statistics in analyzing the images of biological macromolecules. *Ultramicroscopy* 6, 187-194.
- Van Heel M. (1986). Noise-limited three-dimensional reconstructions. *Optik* 73(2), 83-86.
- Van Heel M. (1987). Angular reconstitution: a posteriori assignment of projections for 3D reconstruction. *Ultramicroscopy* 21, 111-124.

# Discussion with Reviewers

**R. Hegerl:** In the context of the scheme of alignment-free classification, each original image is replaced by a half-image containing the amplitudes of the corresponding structure factors and another half-image where a set of invariant phase differences is coded in the form of pixels. To what extent does this non-linear manipulation of images influence the result of classification? Could an adequate weighting of the phase invariants reduce this effect?

**Authors:** The problem mentioned is very serious and well known in pattern recognition. It can be formulated in the following way: how one can mix, in one classification scheme, those features that have different physical units or are measured in arbitrary units? In our case we have two such subsets of features: power spectrum and phases. Unfortunately, this problem does not have a general solution. Rescaling one set of features (parameters) or application of weights changes the result of classification, and thus it has to ap-

### 3-D reconstruction of ice-embedded single particles

plied with caution. Since in our case we subject to classification not the original parameters, but rather factors obtained from the correspondence (principal component) analysis, it means that initially all the parameters are treated as equally important, independently of their scaling.

**J.M.Carazo:** Do you apply some form of phase unwrapping to the proposed phase invariants?

**Authors:** The discussion of the phase unwrapping problem was deliberately omitted from the text. As stated in the text, there are many possibilities to define the phase invariant in a similar fashion. Most of these definitions suffer from the problem that the phases (and operations on them) are defined mod( $2\pi$ ) and the inversion of the parameters derived is not unique. As can be easily verified, the invariants proposed in our paper are uniquely invertible, thus the problem of phase unwrapping does not arise in this context.

**J.M.Carazo:** Please comment on the possible degradations induced by the fact that terms  $\phi(0,1)$  and  $\phi(1,0)$  are not retrieved in image synthesis from phase invariants.

**Authors:** The Fourier transform of the image contains not only the information about the "shape" of the object, but also about its original position in the picture frame. From the point of view of invariant classification, this information is superfluous. In general, the loss of the first phase is equivalent to the loss of information about the original position of the object and does not cause any degradation in the image synthesis. During the image synthesis step, the choice of the first phase will "fix" the position of the retrieved image. In practice, however, the phases  $\phi(0,1)$  and  $\phi(1,0)$  usually correspond to a "non-integer" shift, i.e., a shift by a fraction of the pixel. This means that during the retrieval step an interpolation is implicitly assumed, and this interpolation can cause certain distortions (usually negligible, since much lower than noise).

**J.M.Carazo:** With respect to the fitting of the cones, which I find extremely interesting, could you please comment if the tilt requirement of only  $30^\circ$  comes out from real data testing or from calculations?

**Authors:** We have looked for a scheme that would allow the use of data with tilts as low as  $30^\circ$  because of the difficulties we encountered in trying to obtain high-tilt EM pictures of ice-embedded specimen. Our experience shows that it is relatively easy to obtain good pictures with a tilt lower than  $40^\circ$ . The lower the tilt the lower the defocus spread across the micrograph and, presumably, the better the quality of the reconstruction. At the same time low tilt data supplies a rather limited amount of information (in terms of filling the Fourier space). Thus, a certain balance has to be struck between the feasibility to obtain the pictures at a given tilt, the number of particles which can be collected, the number of preferred orientations in which the particle can be found, and the overall noise level in the data. Thus far we have not been able to test the alignment of experimental  $30^\circ$ -projection sets, because the data sets available were too small and of insufficient quality.

However, we were able to align one of these  $30^\circ$  data sets with the existing  $50^\circ$  data sets (Frank et al., 1991) without difficulty.

**M. van Heel:** SNR's between 1 and 3 were used in the model experiment. With which SNR value is the 85% agreement "with the known origin of the images" associated? -- Since the method is translationally invariant, I really do not understand what such an 85% agreement means.

**Authors:** Since the model used is a 2-D step function, the SNR of the test images (measured as the ratio of amplitudes) is locally strongly varying, namely between 1 and 3. The overall SNR of the test images (expressed in terms of the signal to noise variance) is 1.5. -- With "origin of the images" we mean their "source" or "nature", namely either with or without phase scrambling. We don't refer to the origin of their coordinate system.

The experiment described in the text is the classical experiment to verify the "classification power" of the parameters derived from the data (in our case the shift invariants derived from the 2D images). We know that the images belong to two classes and we know the correct classification. Then we apply cluster analysis (HAC) to the whole data set using factors from the correspondence analysis as parameters. Assuming the existence of two classes we check to which extent the classification obtained agrees with the initial, known classification. The 50% agreement would mean that classification was in fact random and 100% would mean perfect agreement. 85% agreement means that in 85 cases out of 100 the image was assigned to the correct group.

**M. van Heel:** In your "random-conical tilt" technique two images are needed to determine the Euler angles of your 3D reconstruction problem. However, the transfer of the rotational and translational

parameters from the  $0^\circ$  image to the tilted one is associated with experimental errors which could be particularly tricky for ice-embedded specimens since the ice-layer and the molecules may change during the exposures. To what extent do these experimental errors affect the reconstruction results?

**Authors:** It is certainly true that the Euler angles of the tilted images are known only indirectly - through the alignment of the  $0^\circ$  images. Any errors made during the alignment of untilted data will be eventually transferred to the reconstructed object. However, the "quality" of the 3D structure obtained can be estimated by the phase-residual consistency test between the average of untilted images (not used in the 3D reconstruction) and the projection of the structure in the corresponding direction. Our recent results of the ice-embedded data show that it is possible to obtain a resolution of the 3D object (at least in the direction perpendicular to the direction of the missing cone) that matches the resolution of the untilted-particle average - which currently lies in the range of 1/30 to 1/35 Å<sup>-1</sup>. This resolution is limited by a number of factors not all related to the alignment accuracy; among these the high defocus setting and the variations in orientation, see below.

M. van Heel: Along the same line of reasoning: your 3D reconstruction method is based strictly on preferred orientations which probably never really exist (due to the variations in the support film for example). An angular spread of some  $8-10^\circ$  within each "preferred" orientation may be a reasonable estimate. Will this type of error hinder the possibility of reaching high resolution (better than 1nm) with this approach?

Authors: An angular spread of  $8-10^\circ$  within each "preferred" orientation (described as "rocking"), an assumption which we agree seems reasonable, would cause degradation of the resolution of the corresponding  $0^\circ$  average. If we assume the radius of the particle to be  $125 \text{ \AA}$  (e.g., corresponding to the size of the 70S *E.coli* ribosome), then a rotation of the particle by  $10^\circ$  would change the radius of the  $0^\circ$  projection to  $123 \text{ \AA}$ . For a pixel size of  $0.2 \text{ nm}$  (i.e., about half the size we currently use) an angular spread of  $10^\circ$  in the "preferred" orientation would be at the limit of possible detection: such an error in the Euler angle in the projection data would be reflected in a rotation of the particle's periphery by  $.21 \text{ nm}$ , and thus this seems to be the limit of possible resolution for the current data collection scheme and image processing methods. A substantial improvement in resolution can be achieved through improvements in EM data collection (e.g., energy filtration, spot scanning, use of images with different defocus, and collection of larger numbers of particles) that reduce instabilities and improve the signal to noise ratio. Higher-quality data will allow a cyclic refinement of the orientation for individual projections against the entire projection set. Ultimately, a resolution of  $1 \text{ nm}$  appears feasible.

M. van Heel: I agree with the authors that a cross-common-line approach is a more sensible approach than the alignment between 3D reconstructions, each of which associated with a different missing cone area. However, I object to the claims of novelty issued by these authors since the cross-common lines alignment between two sets of projections was already discussed in the very first papers by Crowther et al. in the early seventies. The problem described in those early papers was the relative alignment of two sets of symmetry related projections relative to each other. A new implementation of this idea remains interesting since it may differ in details (the matter is indeed complex) from the earlier ones, yet the claim of novelty is not justified and should be removed from the paper.

Authors: Crowther clearly conceived the use of multiple common lines in finding the orientation between two spherical virus particles seen in projection. An appropriate reference to Crowther et al. (1971) has now been added to the fundamental (1970) reference. The analogy between this method of "cross common lines" and the method we put forth is rather abstract but nevertheless illuminating. In Crowther's application, the "set of projections" is intrinsically fixed to a single virus particle, and the members of that set are related by symmetry. (Incidentally, Crowther et al. (1971) did in fact not use the cross common

lines method to find the orientation, but rather to refine the scaling between the two particles.) In our case, the set of projections corresponds to a set of as many unrelated particles which are deliberately (by inference from an alignment of  $0^\circ$ -degree companion projections) brought into a common coordinate system. Thus the two ideas have a rather complex relationship, and ours is certainly not just a derivative of the other. The wording "put forward" is appropriate, and makes no claim of extraordinary novelty.

M. van Heel: Why is the first factor "responsible for the differences between the two classes", and why is only this factor used for the hierarchical clustering program? (A subjective choice?) Moreover, why is the first eigen-image not similar to the input images, or is this actually the second CORAN eigen-image?

Authors: In our counting, the zero-th factor is associated with the average image. The first eigen-image is in fact similar to the average of one of the sets of invariants, and because of this similarity we used the first factor exclusively for classification.

M. Van Heel: Goncharov, 1986 is a "preprint"? Either refer to published work, to work submitted for publication, or to private communication whichever is appropriate.

Authors: This is the only complete version of Goncharov's work on common lines and moments. It was published in Russian by offset printing in an edition of 200. The cover page identifies this brochure with a (printed!) Russian word that renders the English word "preprint" in a phonetic form. Thus the precise nature of this manifestation of Goncharov's work cannot be captured by any known bibliographic term, because it involves a contradiction of terms. The only precedent for a similar (albeit deliberate) conceptual confusion we are aware of occurs in the realm of Art: Rene Magritte's painting "Ce n'est pas une pipe". In order to convey some of this uncertainty, we have now surrounded the term "preprint" by quotation marks.